BIOCHEMISTRY
including biophysical chemistry & molecular biology
Article

Biochemistry **2009,** *48,* 11097–11107 11097
DOI: 10.1021/bi901179r

Effect of Trans Unsaturation on Molecular Organization in a Phospholipid Membrane[†]

Smita P. Soni,[‡] Jesse A. Ward,[§] Stephanie E. Sen,[∥,@] Scott E. Feller,[§] and Stephen R. Wassall*[,‡,⊥]

[‡]*Department of Physics, Indiana University Purdue University Indianapolis, 402 North Blackford Street, Indianapolis, Indiana 46202-3273,* [§]*Department of Chemistry, Wabash College, Crawfordsville, Indiana 47933,* [∥]*Department of Chemistry and Chemical Biology, Indiana University Purdue University Indianapolis, 402 North Blackford Street, Indianapolis, Indiana 46202-3274, and* [⊥]*Center for Membrane Biosciences, Indiana University Purdue University Indianapolis, 402 North Blackford Street, Indianapolis, Indiana 46202-3274.* [@]*Present address: Department of Chemistry, The College of New Jersey, P.O. Box 7718, Ewing, NJ 08628-0718.*

Received July 10, 2009; Revised Manuscript Received October 9, 2009

ABSTRACT: We employed solid state ^{2}H NMR, complemented by computer simulations, to compare molecular organization in model membranes composed of 1-elaidoyl-2-stearoylphosphatidylcholine (*t*18:1-18:0PC), 1-oleoyl-2-stearoylphosphatidylcholine (*c*18:1-18:0PC), and 1,2-distearoylphosphatidylcholine (18:0-18:0PC). These phospholipids have elaidic acid (EA) containing a trans double bond, oleic acid (OA) containing a cis double bond, and saturated stearic acid (SA), respectively, at the *sn*-1 position and were synthesized with perdeuterated SA at the *sn*-2 position. The temperature of the chain melting transition is depressed less for *t*18:1-18:0PC (31.5 °C) than *c*18:1-18:0PC (7 °C) relative to 18:0-18:0PC (53 °C), reflecting the smaller deviation from the linear conformation produced by a trans as opposed to cis double bond. Acyl chain order in *t*18:1-18:0PC ($\bar{S}_{CD}$ = 0.135) in the liquid crystalline state is much closer to that of *c*18:1-18:0PC ($\bar{S}_{CD}$ = 0.128) than that of the substantially more ordered 18:0-18:0PC ($\bar{S}_{CD}$ > 0.156), which is attributed to the reduced energy barrier to rotation about the C−C single bonds next to either a trans or cis carbon double bond. A conformation that somewhat resembles a saturated chain and an intrinsic disorder approaching that of a cis unsaturated chain characterize EA and, we speculate, may play a role in the adverse impact dietary trans fatty acids (TFA) have on biological function.

Trans fatty acids (TFA)[1] produced during the partial hydrogenation of vegetable oils make up a class of unsaturated fatty acid currently attracting a great deal of attention (*1*, *2*). These "man-made" fatty acids that have become an insidious component in contemporary nutrition (*3*, *4*) adversely affect health, such as increasing the risk of coronary heart disease (*4*, *5*), the development of diabetes (*6*), and colorectal and other cancers (*7*, *8*), by a mechanism that remains to be established. They possess one or more trans double bonds that place the two hydrogen atoms on the opposite side of the double bond, instead of on the same side which occurs in physiologically prevalent cis double bonds (Figure 1). This apparently subtle modification in molecular structure causes a reduction in protein function (*9*) and induces abnormal morphology (*10*) in membranes when TFA-containing lipids replace their cis counterpart. The implication is that changes in the architecture of plasma membranes following incorporation into phospholipids may contribute to the detrimental impact upon health of dietary TFA (*11*−*13*).

Because of the distinction in the geometric disposition of the hydrogen atoms, the torsional states preferred by the single bonds next to a trans or cis double bond differ markedly (*14*). The energy-minimized structure obtained by gas phase ab initio calculations for elaidic acid (EA, *t*18:1), the simplest TFA with a single trans double bond between carbons 9 and 10, deviates much less than oleic acid (OA, *c*18:1), its cis counterpart, from the linear configuration adopted by stearic acid (SA, 18:0) that is the corresponding saturated chain (*15*). Although modeling a free fatty acid oversimplifies the situation in a bilayer, the inference is that a trans double bond will pack more favorably than a cis double bond, resulting in greater stability for the gel state and a smaller reduction in the temperature T_m for the chain melting transition. The T_m values measured for EA-, OA-, and SA-containing phosphatidylcholines (PC) support this view (*16*). Predicting the effect of trans unsaturation on acyl chain organization in the biologically relevant liquid crystalline phase is less straightforward. There are two contrary schools of thought advocating similarity to saturated and cis-unsaturated chains. On one hand, a trans double bond produces a minor discontinuity in the linear conformation adopted by a saturated chain (*15*). On the other hand, and as for a cis double bond (albeit subject to different torsional constraints), rotation about a trans double bond is prohibited while the energy barrier to rotation about the immediately adjacent single bonds is reduced relative to that of a saturated chain (*14*). Two computer simulations of 1-palmitoyl-2-elaidoylphosphatidycholine (16:0-*t*18:1PC) that provide the only order profiles reported to date within trans unsaturated bilayers do not resolve the issue. Close resemblance to 1,2-dipalmitoylphosphatidylcholine (16:0-16:0PC) was revealed by Langevin dynamics in the one case (*17*) and to 1-palmitoyl-2-oleoylphosphatidylcholine (16:0-*c*18:1PC) in the other by

[†]This work was supported by a grant from the American Chemical Society Petroleum Research Fund (43281-AC7) and an award from the National Science Foundation (MCB-0543124).

*To whom correspondence should be addressed. E-mail: swassall@iupui.edu. Telephone: (317) 274-6908. Fax: (317) 274-2393.

[1]Abbreviations: TFA, trans fatty acid(s); CFA, cis fatty acid(s); EA, elaidic acid; OA, oleic acid; SA, stearic acid; PC, phosphatidylcholine(s); PUFA, polyunsaturated fatty acid(s); DPH, 1,6-diphenylhexatriene; AS, anthroyloxystearic acid; MD, molecular dynamics; *t*18:1-18:0PC, 1-elaidoyl-2-stearoylphosphatidylcholine; *c*18:1-18:0PC, 1-oleoyl-2-stearoylphosphatidylcholine; 18:0-18:0PC, 1,2-distearoylphosphatidylcholine.

Published on Web 10/09/2009

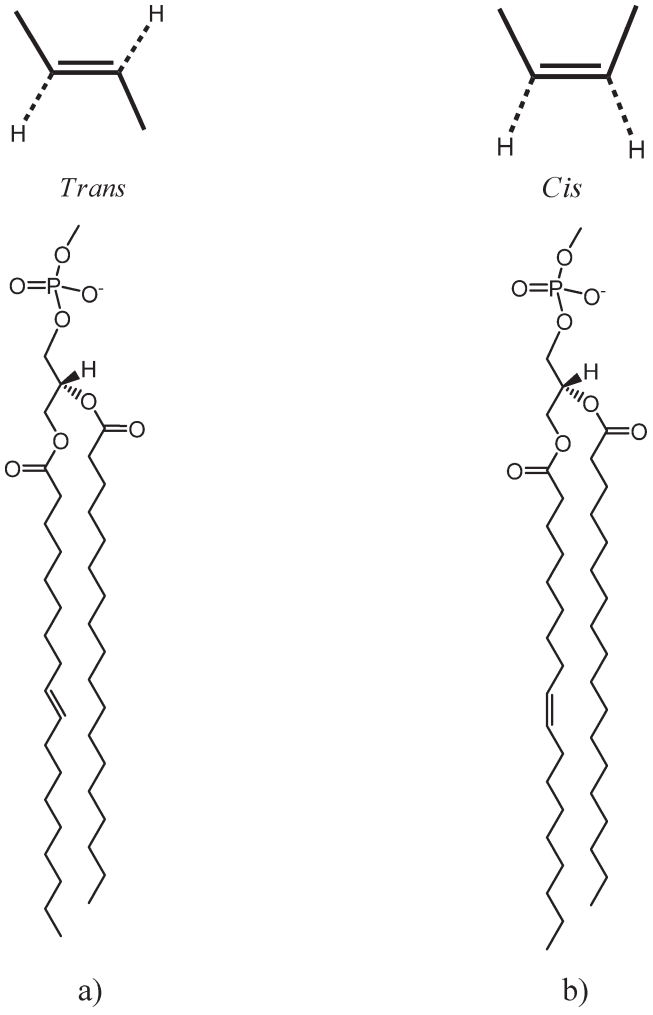

FIGURE 1: Molecular structures of (a) *t*18:1-18:0PC and (b) *c*18:1-18:0PC. The dashed lines emphasize the distinction in configuration between trans and cis double bonds.

molecular dynamics (MD) simulation (*18*). The findings from a sparse collection of experimental studies are equally inconclusive. Steady state fluorescence polarization of DPH (1,6-diphenylhexatriene) and AS (anthroyloxystearic acid) probes indicated that 18:0-*t*18:1PC bilayers are less fluid than 18:0-*c*18:1PC bilayers (*16*). There is, in contrast, negligible difference between average order parameters $\bar{S}_{CD}$ derived for the *sn*-1 chain from ^{2}H NMR spectra for [$^2H_{35}$]18:0-*t*18:1PC (*19*) and [$^2H_{35}$]18:0-*c*18:1PC (*20*).

A solid state ^{2}H NMR spectroscopy study, complemented by atomistic MD calculations, of molecular organization in 1-elaidoyl-2-[$^2H_{35}$]stearoylphosphatidylcholine (*t*18:1-[$^2H_{35}$]-18:0PC) bilayers is presented here. This molecule was chosen because EA is highly abundant in partially hydrogenated vegetable oils (PHVO) (*4*, *21*) and, unlike cis fatty acids (CFA) that usually incorporate as the *sn*-2 chain (*22*), preferentially substitutes at the *sn*-1 position normally occupied by a saturated chain (*4*, *23*−*25*). Perdeuterated [$^2H_{35}$]18:0 acid was esterified at the *sn*-2 position to allow essentially noninvasive observation. Comparison was made with 1-oleoyl-2-[$^2H_{35}$]stearoylphosphatidylcholine (*c*18:1-[$^2H_{35}$]18:0PC). Figure 1 shows the molecular structures of both *t*18:1-18:0PC and *c*18:1-18:0PC. The experiments represent the first direct comparison of TFA- versus CFA-containing phospholipids, which are otherwise identical, that does not rely on a perturbing extrinsic probe.

EXPERIMENTAL PROCEDURES

Materials. *t*18:1-[$^2H_{35}$]18:0PC, as a custom synthesis, and 1-acyl-2-hydroxyphosphatidycholines (18:0lysoPC and *c*18:1lysoPC) were purchased from Avanti Polar Lipids (Alabaster, AL). Cambridge Isotope Laboratories (Andover, MA) and Sigma Chemical Co. (St. Louis, MO) were the source of [$^2H_{35}$]18:0 acid and deuterium-depleted water, respectively.

Synthesis of Deuterated PCs. 18:0-[$^2H_{35}$]18:0PC and *c*18:1-[$^2H_{35}$]18:0PC were synthesized using the method described by Sun et al. (*26*), with a few minor changes. The synthesis was accomplished via dicyclohexylcarbodimide (DCC, 0.8 mmol) coupling of [$^2H_{35}$]18:0 acid (0.4 mmol) with the appropriate lysoPC (0.2 mmol) in the presence of *N*,*N*-dimethylaminopyridine (DMAP, 0.8 mmol) dissolved in dry, distilled chloroform (4 mL). The mixture was stirred for 72 h under an argon atmosphere, and following concentration, the residue was purified by flash chromatography on silica gel in a chloroform/methanol/water (58/35/4, v/v/v) solvent system to give the desired product (80% yield). ^{1}H NMR in C^{2}HCl$_3$ at 500 MHz was performed to confirm the product, which was further purified by HPLC with a reverse-phase silica C18 column (methanol solvent). Molecular masses (825.36 for 18:0-[$^2H_{35}$]18:0PC and 823.34 for *c*18:1-[$^2H_{35}$]18:0PC) were confirmed by liquid chromatography and mass spectrometry (LC−MS).

NMR Sample Preparation. *t*18:1-[$^2H_{35}$]18:0PC, *c*18:1-[$^2H_{35}$]18:0PC, or 18:0-[$^2H_{35}$]18:0PC (60−90 mg) was thoroughly vortex mixed with an equal weight (60−90 μL) of 50 mM Tris buffer (pH 7.5) at a temperature above the gel to liquid crystalline phase transition for each phospholipid. Deuterium-depleted water (~2 mL) was added to the mixture to allow measurement of the pH which was adjusted to 7.5. Three lyophilizations in the presence of excess deuterium-depleted water were then performed to remove naturally abundant ^{2}HHO. After a final hydration to 50 wt %, the resultant sample was transferred to a 5 mm NMR tube that was sealed with a Teflon-coated plug. It was stored at −80 °C and equilibrated at room temperature before the experiments.

^{2}H NMR Spectroscopy. Solid state ^{2}H NMR experiments were performed on a home-built spectrometer operating at 27.6 MHz with a 4.2 T Nalorac superconducting magnet (*27*). A desktop computer controlled the spectrometer. Pulse programming was accomplished using an in-house assembled programmable pulse generator with a design based upon an Am2910 processor (Advanced Micro Devices, Sunnyvale, CA) (*28*), while signals were acquired in quadrature using a Rapid Systems (Seattle, WA) R1200M dual-channel digital oscilloscope. Sample temperature was regulated to ±0.5 °C by a Love Controls (Michigan City, IN) 1600 Series temperature controller. A phase-alternated quadrupolar echo sequence $(90°_x-\tau-90°_y-\text{acquire}-\text{delay})_n$ that eliminates spectral distortion due to receiver recovery time was implemented to collect spectra (*29*). Unless otherwise stated, spectral parameters were as follows: 90° pulse width, ≈4 μs; separation between pulses (τ), 50 μs; delay between pulse sequences, 1.0 s (gel phase) or 1.5 s (liquid crystalline phase); sweep width, ±250 kHz (gel phase) or ±100 kHz (liquid crystalline phase); data set, 2K points; number of transients, 1024.

Analysis of ^{2}H NMR Spectra. First moments (M_1) (*30*) were calculated from the powder pattern spectra with

$$M_1 = \frac{\int_{-\infty}^{\infty} |\omega| f(\omega)\, d\omega}{\int_{-\infty}^{\infty} f(\omega)\, d\omega} \quad (1)$$

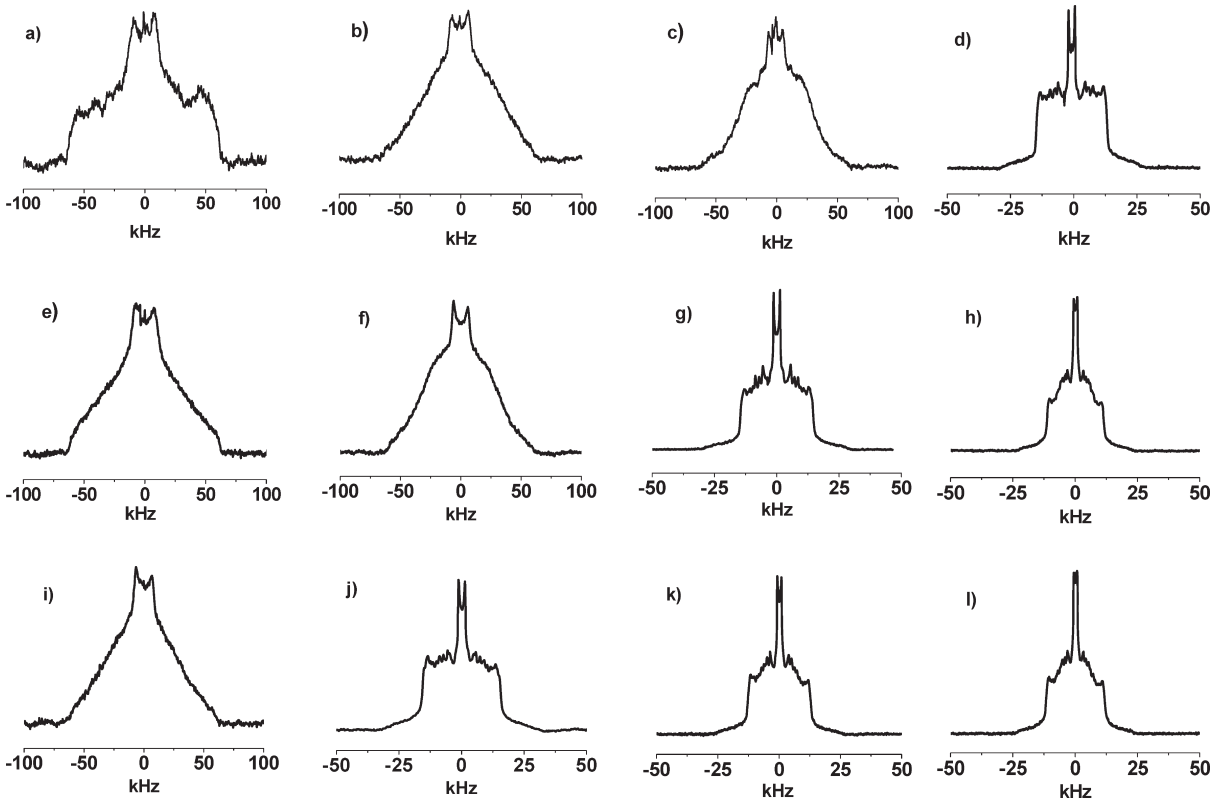

FIGURE 2: ^{2}H NMR spectra for 50 wt % aqueous dispersions in 50 mM Tris (pH 7.5) of (a−d) 18:0-[$^2H_{35}$]18:0PC, (e−h) *t*18:0-[$^2H_{35}$]18:0PC, and (i−l) *c*18:1-[$^2H_{35}$]18:0PC. The spectra were recorded at (a, e, and i) −5 °C, (b, f, and j) 20 °C, (c, g, and k) 45 °C, and (d, h, and l) 60 °C.

where $f(\omega)$ represents the line shape as a function of frequency ω relative to the central Larmor frequency ω_0. In practice, the integration was a summation over the digitized data. The value of M_1 is a sensitive indicator of membrane phase and equates via the static quadrupolar coupling constant [$(e^2qQ)/h$ = 167 kHz] to an average order parameter $\bar{S}_{CD}$ for the perdeuterated [$^2H_{35}$]18:0 *sn*-2 chain in the liquid crystalline state according to

$$M_1 = \frac{\pi}{\sqrt{3}}\left(\frac{e^2qQ}{h}\right)|\bar{S}_{CD}| \quad (2)$$

The FFT depaking algorithm was applied to deconvolute the powder pattern signal to an aligned spectrum representative of a planar bilayer to further elaborate order within the liquid crystalline bilayer (*27*). The depaked spectrum consists of doublets with quadrupole splittings $\Delta\nu(\theta)$ that relate to order parameters S_{CD} by

$$\Delta\nu(\theta) = \frac{3}{2}\left(\frac{e^2qQ}{h}\right)|S_{CD}|P_2(\cos\theta) \quad (3)$$

where θ = 0° is the angle the normal to the membrane surface makes with the magnetic field and $P_2(\cos\theta)$ is the second-order Legendre polynomial. A smoothed profile of order parameter was generated then on the basis of integrated intensity assuming monotonic variation toward the terminal methyl in the disordered center of the membrane (*31*).

MD Simulations. MD simulations for *t*18:1-18:0PC and *c*18:1-18:0PC bilayers at 45 °C with a duration of 5 ns were conducted using eight processors on a Beowulf-type parallel computer. Each simulation cell contained 72 lipids (36 per monolayer) and 1930 waters, corresponding to full hydration. The Chemistry at HARvard Molecular Mechanics (CHARMM) program (*32*) was employed with the PARAM22b4b all-atom parameter set (*33*) and its extension to cis-unsaturated lipids (*34*), while a new set was developed for the EA chain by previously described methods (*34*). We took initial conformations from the end of previously equilibrated simulations by applying restraints to the double bond torsions to produce the desired conformers during energy minimization. Electrostatic interactions were introduced via the particle mesh Ewald summation (*35*). All bonds involving hydrogen were fixed at their equilibrium distances with the SHAKE algorithm (*36*). The time step was 2 fs, implemented with a leapfrog Verlet integration scheme. A flexible simulation cell was used with the *z* dimension (bilayer normal) adjusted to maintain P_{zz} = 1 atm, and the *x* and *y* dimensions were adjusted to maintain a surface area of 65.9 Å^2/molecule. The fixed area ensemble was chosen to ensure that the molecular areas were consistent with experiment. The number of lipids in the simulation cell, while smaller than those in some studies, has been used in a number of published reports from our laboratory that were successfully used to aid in the interpretation of NMR experiments and has been shown to be more than adequate for the computation of equilibrium structural properties (*37*). Coordinates were saved every picosecond for subsequent analysis that included the calculation of order parameters.

RESULTS

^2H NMR. Solid state ^{2}H NMR spectra for 50 wt % aqueous dispersions of *t*18:1-18:0[$^2H_{35}$]PC, *c*18:1-18:0[$^2H_{35}$]PC, and, as the saturated control, 18:0-18:0[$^2H_{35}$]PC in 50 mM Tris (pH 7.5) were recorded as a function of temperature to investigate the changes that EA versus OA causes to phase behavior and membrane organization.

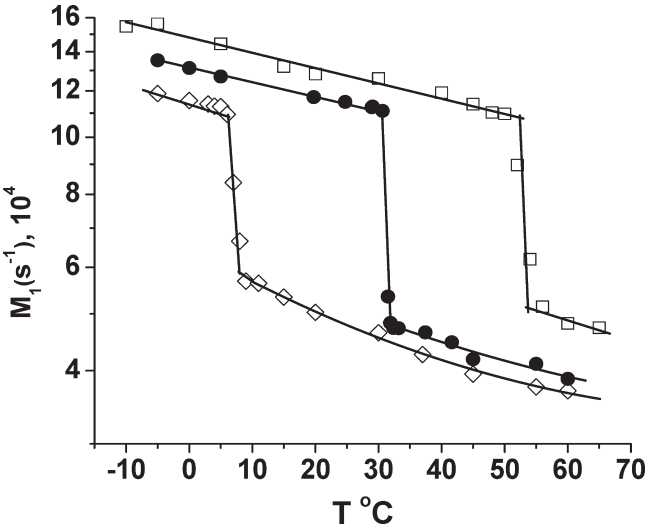

FIGURE 3: Variation of the first moment (M_1) as a function of temperature for 18:0-[$^2H_{35}$]18:0PC (□), *t*18:0-[$^2H_{35}$]18:0PC (●), and *c*18:1-[$^2H_{35}$]18:0PC (◇). M_1 is plotted logarithmically for the sake of clarity. The values given for the transition temperature T_m in Table 1 are the midpoint of the sharp drop in moment that accompanies chain melting.

(*i*) *Phase Behavior*. Representative examples of spectra at selected temperatures for 18:0-18:0[$^2H_{35}$]PC, *t*18:0-18:0[$^2H_{35}$]PC, and *c*18:1-18:0[$^2H_{35}$]PC are shown in Figure 2. The dramatic narrowing of the spectral shape that accompanies the melting of acyl chains at the transition between gel and liquid crystalline states is apparent for each phospholipid, and inspection reveals differences in the effect of EA and OA on membrane phase behavior. All three phospholipids exhibit spectra characteristic of the lamellar gel phase at −5 °C (Figure 2a,e,i), the lowest temperature, and of the lamellar liquid crystalline phase at 60 °C (Figure 2d,h,l), the highest temperature (*30*, *38*). In the gel phase, the [$^2H_{35}$]18:0 *sn*-2 chains are rigid and their slow rotational diffusion confers nonaxial symmetry on a featureless broad spectrum with shoulders at ±63 kHz (Figure 2a,e,i). Rapid isomerization about C−C bonds in the [$^2H_{35}$]18:0 *sn*-2 chain is responsible in the liquid crystalline phase for a much narrower spectrum with well-defined edges at approximately ±15 kHz that correspond to the plateau region of relatively constant order in the upper part of the chain (Figure 2d,h,l). The individual peaks within the spectrum arise from less ordered methylenes in the lower part of the acyl chain, and the highly mobile terminal methyl is represented by a central pair of peaks. Between the two extreme temperatures, differences in phase behavior become evident in the spectra. The spectra for 18:0-18:0[$^2H_{35}$]PC (Figure 2b) and *t*18:0-18:0[$^2H_{35}$]PC (Figure 2f) remain gel-like at 20 °C, while that for *c*18:1-18:0[$^2H_{35}$]PC (Figure 2j) indicates that the CFA-containing membrane has become liquid crystalline. Upon a further 25 °C increase in temperature to 45 °C, TFA-containing *t*18:0-18:0[$^2H_{35}$]PC (Figure 2g) as well as *c*18:0-18:0-[$^2H_{35}$]PC (Figure 2k) exhibits a spectrum typical of the liquid crystalline state, and only for disaturated 18:0-18:0[$^2H_{35}$]PC (Figure 2c) does the spectrum imply the gel phase.

The spectra presented in Figure 2 are examples of spectra that were acquired over a span in temperature from −10 to 65 °C. They illustrate the sensitivity of spectral line shape to membrane phase. The first moment, M_1, defined by eq 1, offers a method of quantifying the shape and monitoring phase behavior when plotted against temperature (*26*). Figure 3 presents M_1 as a function of temperature for *t*18:1-[$^2H_{35}$]18:0PC, *c*18:1-[$^2H_{35}$]-18:0PC, and 18:0-[$^2H_{35}$]18:0PC. There are two ranges of temperature for each PC in which M_1 values vary slowly separated by an abrupt discontinuity. In the case of *t*18:1-[$^2H_{35}$]18:0PC (●), the gel phase is signified by an M_1 of $> 11.1 \times 10^4$ s^{-1} below 30.5 °C while the liquid crystalline state characterized by an M_1 of $< 4.8 \times 10^4$ s^{-1} above 32.5 °C. A similar discontinuity is seen at lower temperatures for *c*18:1-[$^2H_{35}$]18:0PC (◇), where an M_1 of $> 10.9 \times 10^4$ s^{-1} and an M_1 of $< 5.7 \times 10^4$ s^{-1} signify the gel phase below 6 °C and the liquid crystalline state above 9 °C, respectively. In the saturated lipid, 18:0-[$^2H_{35}$]18:0PC (□), the moments ($M_1 > 11.0 \times 10^4$ s^{-1}) remain symptomatic of the gel state until 50 °C and then the liquid crystalline is indicated by an M_1 of $< 5.1 \times 10^4$ s^{-1} for temperatures in excess of 56 °C.

The dramatic drop in the value of M_1 corresponds to the tremendous change in line shape that accompanies acyl chain melting when the lipid undergoes the transition from the gel to liquid crystalline state. It is clear from the plots in Figure 3 that the temperature at which *t*18:1-[$^2H_{35}$]18:0PC melts lies approximately midway between those for 18:0-[$^2H_{35}$]18:0PC and *c*18:1-[$^2H_{35}$]18:0PC. The values for the temperature of the phase transition T_m derived from the center of the discontinuity in each plot are given in Table 1. For the lipid with a SA *sn*-1 chain, the T_m equals 53.0 °C, which is much higher than the T_m of 7.0 °C for the lipid with an OA *sn*-1 chain. In between at 31.5 °C is the T_m for the lipid with an EA *sn*-1 chain.

(*ii*) *Acyl Chain Order*. In the liquid crystalline phase where rapid molecular reorientation results in spectra symptomatic of axially symmetry, the first moment M_1 is related to the average order parameter $\bar{S}_{CD}$ for the entire [$^2H_{35}$]18:0 *sn*-2 chain via eq 2. The values obtained for $\bar{S}_{CD}$ in *t*18:1-[$^2H_{35}$]18:0PC and *c*18:1-[$^2H_{35}$]18:0PC bilayers at 45 °C, together with 18:0-[$^2H_{35}$]18:0PC at 60 °C, are listed in Table 2. They reveal that order is only slightly greater in the EA-containing ($\bar{S}_{CD} = 0.135$) than in the OA-containing ($\bar{S}_{CD} = 0.128$) membrane. In both cases, order is lower than in the saturated membrane where $\bar{S}_{CD} = 0.156$ at 60 °C. The calculation was performed at a higher temperature for 18:0-[$^2H_{35}$]18:0PC because the saturated lipid, unlike *t*18:1-[$^2H_{35}$]18:0PC and *c*18:1-[$^2H_{35}$]18:0PC, is in the gel state at

Table 1: Temperatures (T_m) for the Gel to Liquid Crystalline Phase Transition Determined by Moment Analysis of ^{2}H NMR Spectra

lipid composition	T_m (°C)
18:0-[$^2H_{35}$]18:0PC	53.0
*t*18:1-[$^2H_{35}$]18:0PC	31.5
*c*18:1-[$^2H_{35}$]18:0PC	7.0

Table 2: Average Order Parameters ($\bar{S}_{CD}$) Calculated from the First Moment (M_1) for the [$^2H_{35}$]18:0 *sn*-2 Chain in *t*18:1-[$^2H_{35}$]18:0PC and *c*18:1-[$^2H_{35}$]18:0PC at 45 °C and the Corresponding Values Calculated from MD Simulations[a]

	$\bar{S}_{CD}$	
lipid composition	^{2}H NMR	MD
*t*18:1-[$^2H_{35}$]18:0PC	0.135	0.148
*c*18:1-[$^2H_{35}$]18:0PC	0.128	0.146
18:0-[$^2H_{35}$]18:0PC	0.156	−[b]

[a]A temperature of 60 °C applies to the value of $\bar{S}_{CD}$ stated for 18:0-[$^2H_{35}$]18:0PC. [b]MD simulations were not performed on 18:0-18:0PC.

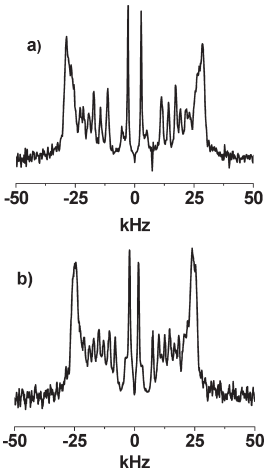

FIGURE 4: FFT depaked spectra for (a) *t*18:1-[$^2H_{35}$]18:0PC and (b) *c*18:1-[$^2H_{35}$]18:0PC at 45 °C.

45 °C. Thus, the data in Table 2 underestimate the differential in order between unsaturated and saturated systems.

To elaborate upon the distribution of order along the chain, the NMR signal was FFT depaked (*27*). Application of this procedure results in a spectrum equivalent to that obtained for a planar membrane with the bilayer normal aligned parallel to the magnetic field, consisting of a superposition of doublets as illustrated in Figure 4 for *t*18:1-[$^2H_{35}$]18:0PC and *c*18:1-[$^2H_{35}$]18:0PC. For each lipid, an outermost composite doublet, representing ordered methylenes in the upper part of the [$^2H_{35}$]18:0 *sn*-2 chain, and a series of well-resolved doublets with smaller splittings, predominantly corresponding to the methylenes and terminal methyl that display progressively less order in the lower portion of the chain, are clearly discernible in the depaked spectrum. The vast enhancement in resolution achieved facilitates the generation of a profile of the order parameter.

The smoothed order parameter profiles shown in Figure 5 for *t*18:1-[$^2H_{35}$]18:0PC and *c*18:1-[$^2H_{35}$]18:0PC membranes (Figure 5a) were created from the depaked spectra (Figure 4) via assignment of equal intensity to each methylene group and assuming a continuous decrease of order toward the terminal methyl (*31*). It should be noted that constraints imposed upon the initial orientation of the *sn*-2 chain render the C2 position an exception to the assumption that order varies monotonically (*39*). The inequivalent S_{CD} values plotted for the two deuterons at this position were calculated from the splittings of doublets that were assigned on the basis of intensity and comparison with work on selectively deuterated PCs (*34*). Inspection of the profiles reveals that they are quite similar for the TFA- and CFA-containing membranes. Apart from the C2 position, there is a characteristic plateau region of slowly decreasing order in each of the lipids in the upper portion of the perdeuterated acyl chain followed in the lower portion by a progressively greater reduction in order toward the bottom of the chain. Slightly higher order in the lower half (C9 onward) of the [$^2H_{35}$]18:0 *sn*-2 chain for the EA-containing (●) than for the OA-containing (◇) membrane is the only difference. Consistent with the values for the average order parameter presented in Table 2, higher order is exhibited throughout the profile for 18:0-[$^2H_{35}$]18:0PC at 60 °C (Figure 5a, solid line) that is also included in Figure 5.

MD Simulations. MD simulations of *t*18:1-18:0PC and *c*18:1-18:0PC bilayers were performed to aid in the interpretation of the NMR data. The advantage of the computer modeling

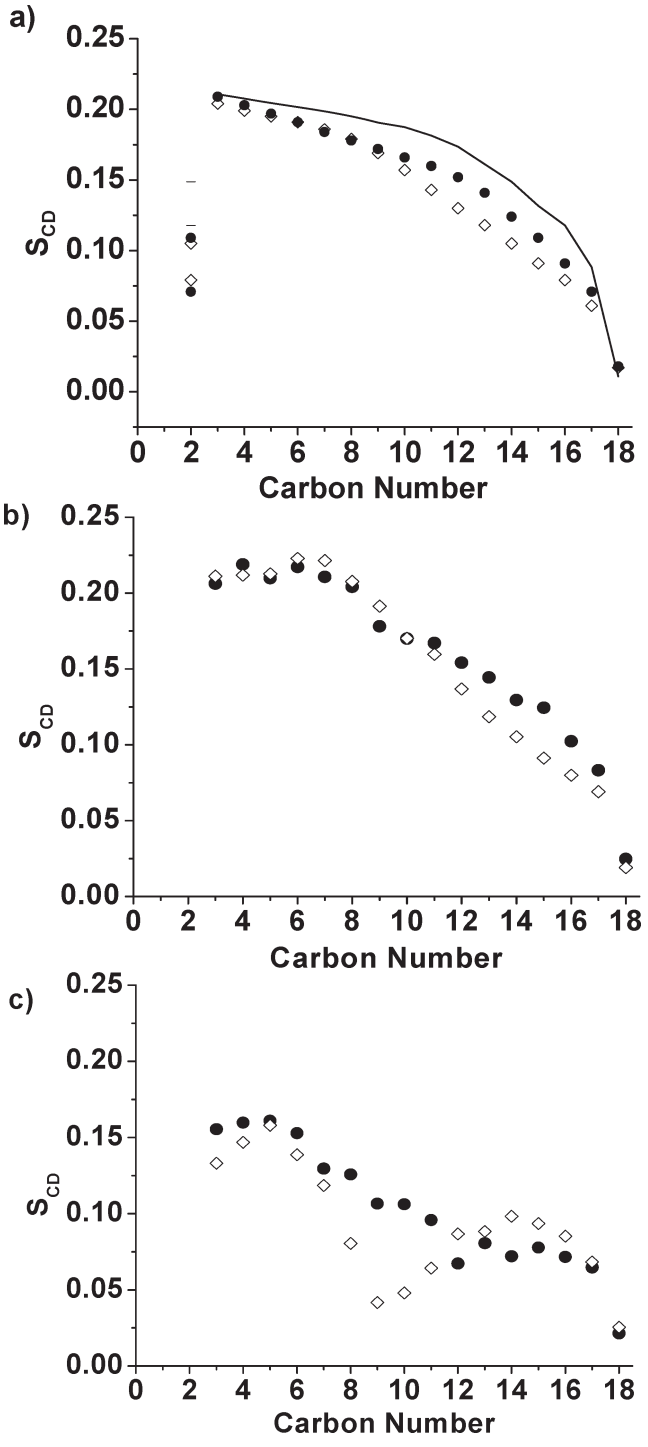

FIGURE 5: Order parameter profiles for *t*18:1-18:0PC (●) and *c*18:1-18:0PC (◇) at 45 °C generated from FFT depaked spectra for (a) the *sn*-2 chain and from MD simulations for (b) the *sn*-2 chain and (c) the *sn*-1 chain. The solid line in panel a is the order parameter profile generated from depaked spectra for the *sn*-2 chain of 18:0-18:0PC at 60 °C.

technique is its ability to provide an atomic-level picture of molecular conformations and temporal dynamics that can only come indirectly from interpretation of experimental data (*40*, *41*). However, validation with experimental results is crucial because simulations require the input of initial conditions and empirically derived expression for force fields. Testing against the S_{CD} values measured by ^2H NMR for the [$^2H_{35}$]18:0 *sn*-2 chain in *t*18:1-[$^2H_{35}$]18:0PC and *c*18:1-[$^2H_{35}$]18:0PC fulfills that purpose here.

The order parameter profiles generated from MD simulations on *t*18:1-18:0PC and *c*18:1-18:0PC are displayed in Figure 5. Table 2 includes the associated values for the value of the average order parameter $\bar{S}_{CD}$. The simulated values of S_{CD} were calculated as a time and ensemble average over trajectories according to

$$S_{CD} = \frac{1}{2}\langle 3\cos^2\beta - 1\rangle \quad (4)$$

In this equation, which serves as the definition of the deuterium order parameter (*42*), β is the instantaneous angle that a C$-^2$H bond vector makes with respect to the bilayer normal and the angular brackets designate a time average. The C2 position was omitted from the calculations in view of the recognized failure of simulations to reproduce experimental order parameters at this location in either the *sn*-1 or -2 chain (*43*). It can be seen that the overall shape of the computationally derived profile for the SA *sn*-2 chain (Figure 5b) possesses good agreement with experiment (Figure 5a). The "signature" plateau region of virtually constant order in the upper part of the chain followed by gradually decreasing order in the lower part is clearly exhibited by the simulated data that, like the experimental data, furthermore reveal slightly less disorder in *t*18:1-18:0PC (●) than *c*18:1-18:0PC (◇) bilayers. There is a trend of somewhat higher order in the simulation for both TFA- and CFA-containing lipids ($\bar{S}_{CD}$ = 0.148 and 0.146, respectively) relative to the ^{2}H NMR data ($\bar{S}_{CD}$ = 0.135 and 0.128, respectively), which we ascribe to a choice for the area per molecule that may be a few percent too low or potentially from incomplete sampling in the finite-length simulation. Another factor is the contribution from the C2 position, where S_{CD} is small, to the NMR-derived data that the simulation does not include.

Order parameters extracted for the EA and OA *sn*-1 chains from the MD simulations for *t*18:1-18:0PC and *c*18:1-18:0PC are also plotted versus carbon number in Figure 5c. Major differences exist in comparison to the gradient of order along the 18:0 *sn*-1 chain. The S_{CD} values for the trans- and cis-unsaturated chains are lower and are not characterized by a region of uniform order in the upper portion. In the case of the *t*-18:1 *sn*-1 chain (●), they gradually decrease throughout the chain toward the terminal methyl end. The small deviations from monotonic variation that are apparent would be expected to disappear in simulations longer in duration. As expected from the geometry of a trans double bond that aligns the C$-$H bonds parallel to each other and confirmed by the single quadrupolar splitting measured for 16:0-[9,10-^{2}H$_2$]*t*18:1PC with selectively deuterated EA in the *sn*-2 chain (*44*), the order parameters at positions 9 and 10 are the same. There is no dramatic dip in S_{CD} value near the trans double bond of the kind seen by simulation in the vicinity of the cis double bond in the OA *sn*-1 chain for *c*18:1-18:0PC [Figure 5c (◇)]. This dip is consistent with the greatly diminished S_{CD} values at the C9, C10, and surrounding positions measured experimentally and computer modeled for OA esterified to the *sn*-2 position in 16:0-*c*18:1PC and *sn*-1 and -2 positions in 1,2-dioleoylphosphatidylcholine (*c*18:1-*c*18:1PC) (*44*$-$*46*). Extremely high disorder within the cis-unsaturated chain is not the reason. When geometrical factors were taken into account, prior analysis of ^{2}H NMR splittings measured for 16:0-[9,10-^{2}H$_2$]*c*18:1PC established that an average orientation close to the bilayer normal for the cis double bond is responsible (*44*).

DISCUSSION

The aim of this work is to elucidate molecular organization within a model membrane comprised of PC molecules in which EA, the simplest and most common TFA, replaces the saturated fatty acid normally found at the *sn*-1 position. Solid state ^{2}H NMR and MD simulations were employed to compare phase behavior and acyl chain order in *t*18:1-18:0PC and, the CFA-containing counterpart, *c*18:1-18:0PC.

EA Packs Better Than OA in the Gel Phase. ^{2}H NMR spectra for *t*18:1-[^{2}H$_{35}$]18:0PC, *c*18:1-[^{2}H$_{35}$]18:0PC, and 18:0-[^{2}H$_{35}$]18:0PC at representative temperatures from a range that spans -5 to 65 °C are presented in Figure 2. In each case, they reveal upon heating a change in spectral shape from entirely characteristic of the gel phase to entirely characteristic of the liquid crystalline phase. The introduction of unsaturation clearly depresses the temperature at which the phase transition occurs, the depression associated with OA exceeding that with EA. Whereas only the spectrum at 60 °C for 18:0-[^{2}H$_{35}$]18:0PC (Figure 2d) signifies the membrane has become liquid crystalline, the spectra at 45 and 60 °C for *t*18:0-[^{2}H$_{35}$]18:0PC (Figure 2g,h) and at 20, 45, and 60 °C for *c*18:1-18:0PC (Figure 2j$-$l) demonstrate that these membranes entered the liquid crystalline state at lower temperature.

The phase behavior of the three membranes is elaborated in Figure 3 by a plot against temperature of first moment M_1 calculated from all the spectra collected. A sharp drop in the value of M_1 that accompanies the melting of the [^{2}H$_{35}$]18:0 *sn*-2 chain is well-defined for *t*18:1-[^{2}H$_{35}$]18:0PC, *c*18:1-[^{2}H$_{35}$]18:0PC, and 18:0-[^{2}H$_{35}$]18:0PC. The midpoint is identified as the transition temperature T_m, and Table 1 lists the values measured. As was surmised by visual inspection of the spectra, T_m is reduced less by a trans than by a cis double bond. The transition temperature for *t*18:1-[^{2}H$_{35}$]18:0PC (31.5 °C) lies midway between those for 18:0-[^{2}H$_{35}$]18:0PC (53.0 °C) and *c*18:1-[^{2}H$_{35}$]18:0PC (7.0 °C). To the best of our knowledge, a transition temperature has not previously been reported for *t*18:1-18:0PC. Values for T_m have been measured by differential scanning calorimetry (DSC) for 18:0-*t*18:1PC (31.1 °C) and 18:0-*c*18:1PC (5.5 °C) where the *sn*-1 and -2 chains are interchanged relative to the current work (*16*). They show the same behavior. Adding a single trans double bond to the *sn*-2 chain, like to the *sn*-1 chain, lowers the transition temperature approximately half as much as a cis double bond. The phase transition temperatures published for homoacid PC with two identical mono-unsaturated chains are predictably much lower than for heteroacid PC with a combination of saturated and mono-unsaturated chains at the *sn*-1 and -2 positions or vice versa. In common with the corresponding heteroacid species, the transition for EA-containing 1,2-dielaidoylphosphatidylcholine (*t*18:1-*t*18:1PC) (T_m = 11.1 °C) is depressed substantially less than that for OA-containing 1,2-dioloeylphosphatidylcholine (*c*18:1-*c*18:1PC) (T_m = -18.1 °C) (*12*). Under physiological conditions where EA replaces a saturated fatty acid such as SA in the *sn*-1 position of phospholipids and is typically paired with an unsaturated CFA in the *sn*-2 position (*25*), a lowering of the transition temperature would result due to a higher degree of unsaturation.

The lowering of the transition temperature for *t*18:1-18:0PC and *c*18:1-18:0PC is attributable to the deviation from a linear conformation that results when a trans and, to a greater degree, cis double bond is introduced into a saturated fatty acid chain. Looser packing and a consequent reduction in intra- and intermolecular van der Waals interactions within the ordered interior of the bilayer in the gel state decrease stability, manifest as a depression of the temperature at which the chains melt. Energy-minimized structures are presented in Figure 6 to illustrate the

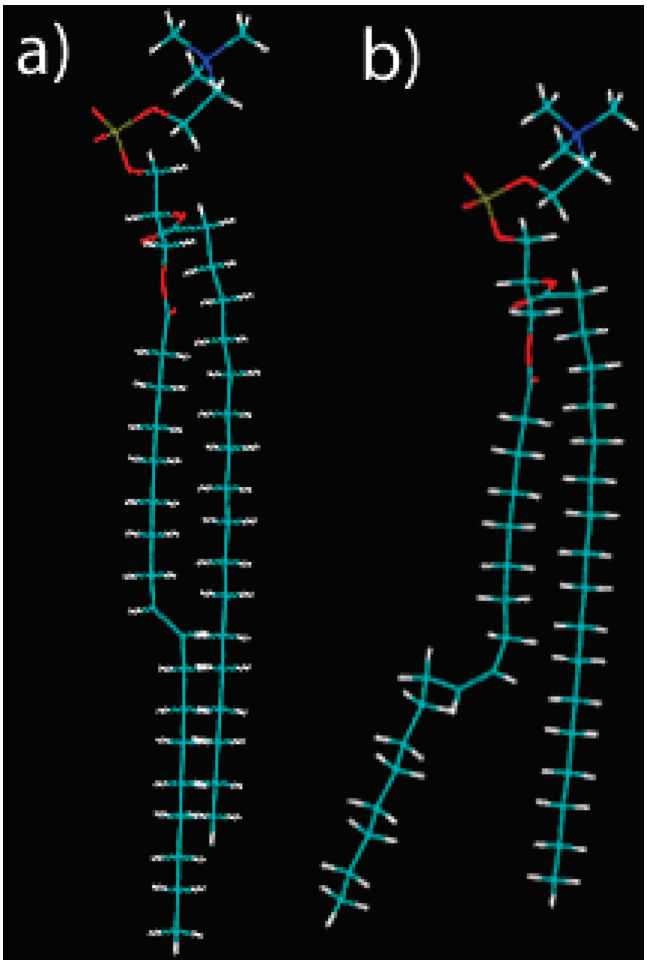

FIGURE 6: Energy-minimized structures for (a) *t*18:1-18:0PC and (b) *c*18:1-18:0PC.

point. The saturated SA chain at the *sn*-2 position in *t*18:1-18:0PC (Figure 6a) or *c*18:1-18:0PC (Figure 6b) is straight. All of the single C−C bonds are in the trans (*t*) conformation. The mono-unsaturated EA (Figure 6a) or OA (Figure 6b) chain at the *sn*-1 position, on the contrary, is kinked. A $ts^{-}\Delta s^{-}t$ or $ts^{-}\Delta s^{-}g^{-}$ sequence of rotational states [$s^{\pm}$ and $g^{\pm}$ specify, correspondingly, skew(±) and gauche(±) conformations] is preferred in the vicinity of the rigid trans or cis double (Δ) bond, respectively. The structure modeled for SA and EA attached to a phospholipid matches the conformation modeled as a free fatty acid. The structure modeled for OA esterified to PC, as discussed by Huang and Li (*47*), includes a trans → gauche isomerization next to the $s^{-}\Delta s^{-}$ sequence to create a crankshaft-like motif as opposed to the twisted boomerang shape modeled as a free fatty acid. That the EA chain in *t*18:1-18:0PC (Figure 6a) has a less accentuated kink and deviates from linearity to a smaller extent than the OA chain in *c*18:1-18:0PC (Figure 6b), and would pack more favorably in the gel state, is evident in the lowest-energy conformers obtained here with individual molecules in the gas phase. Consistent with greater stability, moreover, stronger van der Waals interaction between *sn*-1 and -2 chains is computed using the interaction energy facility in CHARMM for the lowest-energy conformers modeled for the EA-containing PC than for OA-containing PC. The interaction energy is, accordingly, −1.8 versus −0.7 kcal/mol (between carbons 10 and 18 and their associated hydrogens) in the bottom of the chain where EA, unlike OA, lines up close to the SA chain. In the top of the chain where EA and OA adopt a similar conformation, the interaction energy is −2.2 kcal/mol (between carbons 1 and 9) and the same.

EA Disorders Almost as Much as OA in the Liquid Crystalline Phase. The plot of first moment M_1 versus temperature in Figure 3 shows that the M_1 values for *t*18:1-[$^2H_{35}$]18:0PC consistently lie just above (~7%) those for *c*18:1-[$^2H_{35}$]18:0PC and well below (~25%) those for 18:0-[$^2H_{35}$]-18:0PC, when the membranes are examined in the physiologically relevant liquid crystalline state. Invoking the relationship between M_1 and average order parameter $\bar{S}_{CD}$ (eq 2), thus, establishes that introducing a trans or cis double bond increases disorder. Furthermore, order within the EA-containing membrane is much closer to the OA-containing than the disaturated membrane.

Table 2 lists the average order parameters determined from the ^{2}H NMR spectra recorded for *t*18:1-[$^2H_{35}$]18:0PC and *c*18:1-[$^2H_{35}$]18:0PC at 45 °C, which were analyzed in detail for elucidation and comparison of acyl chain organization within the membranes. They confirm the trend gleaned from the moments. While *t*18:1-[$^2H_{35}$]18:0PC ($\bar{S}_{CD}$ = 0.135) is slightly more ordered than *c*18:1-[$^2H_{35}$]18:0PC ($\bar{S}_{CD}$ = 0.128), both membranes possess substantially greater disorder than 18:0-[$^2H_{35}$]18:0PC ($\bar{S}_{CD}$ = 0.153). It should be noted that the $\bar{S}_{CD}$ value for 18:0-[$^2H_{35}$]18:0PC was measured at 60 °C because the disaturated membrane is in the gel phase at 45 °C and, as a point of reference, underestimates the reduction in order produced at the lower temperature when a double bond is introduced. That a trans and cis double bond exert a comparable effect on membrane order is consistent with earlier published ^{2}H NMR work on [$^2H_{31}$]16:0-*t*18:1PC (*19*) and [$^2H_{31}$]16:0-*c*18:1PC (*20*) with EA and OA attached at the *sn*-2 position, respectively. A reservation about this comparison is that it is based upon data collected in two independent studies under experimental conditions that were not necessarily equivalent.

Profiles of order along the saturated [$^2H_{35}$]18:0 *sn*-2 chain in *t*18:1-[$^2H_{35}$]18:0PC and *c*18:1-[$^2H_{35}$]18:0PC membranes that were generated from depaked spectra (Figure 4) to investigate the small differential in average order between the membranes are presented in Figure 5. The general shape for the two membranes is similar (Figure 5a) and matches that universally seen with saturated chains in liquid crystalline phospholipid bilayers (*41*). Except for the C2 position that is constrained in orientation by the glycerol backbone (*38*), order varies monotonically. A plateau region of slowly decreasing order parameter in the upper portion is followed by a progressively more rapid decrease toward the terminal methyl in the lower portion. The plateau region of almost constant order is due to a predominance of trans rotational isomeric states aligning segments parallel to the bilayer normal, together with approximately constant probability for conformations with other orientations, in the upper portion of the chain (*48*). In the lower portion, a decrease in number of trans segments oriented parallel to the bilayer normal is responsible for the loss of order. Figure 5 reveals that slightly higher order below the C9 position in the EA-containing membrane, which extends the plateau region in *t*18:1-[$^2H_{35}$]18:0PC (C3−C11) relative to *c*18:1-[$^2H_{35}$]18:0PC (C3−C9), is the origin of the difference in the value of $\bar{S}_{CD}$ determined with the two types of mono-unsaturated membranes (Table 2). Above the C9 position, the profiles are almost identical. Comparison with the plateau region (C3−C11) in the profile for 18:0-[$^2H_{35}$]18:0PC (Figure 5a, solid line) indicates that the disordering caused by a trans double bond does not entail the shortening of the plateau region associated with a cis double bond.

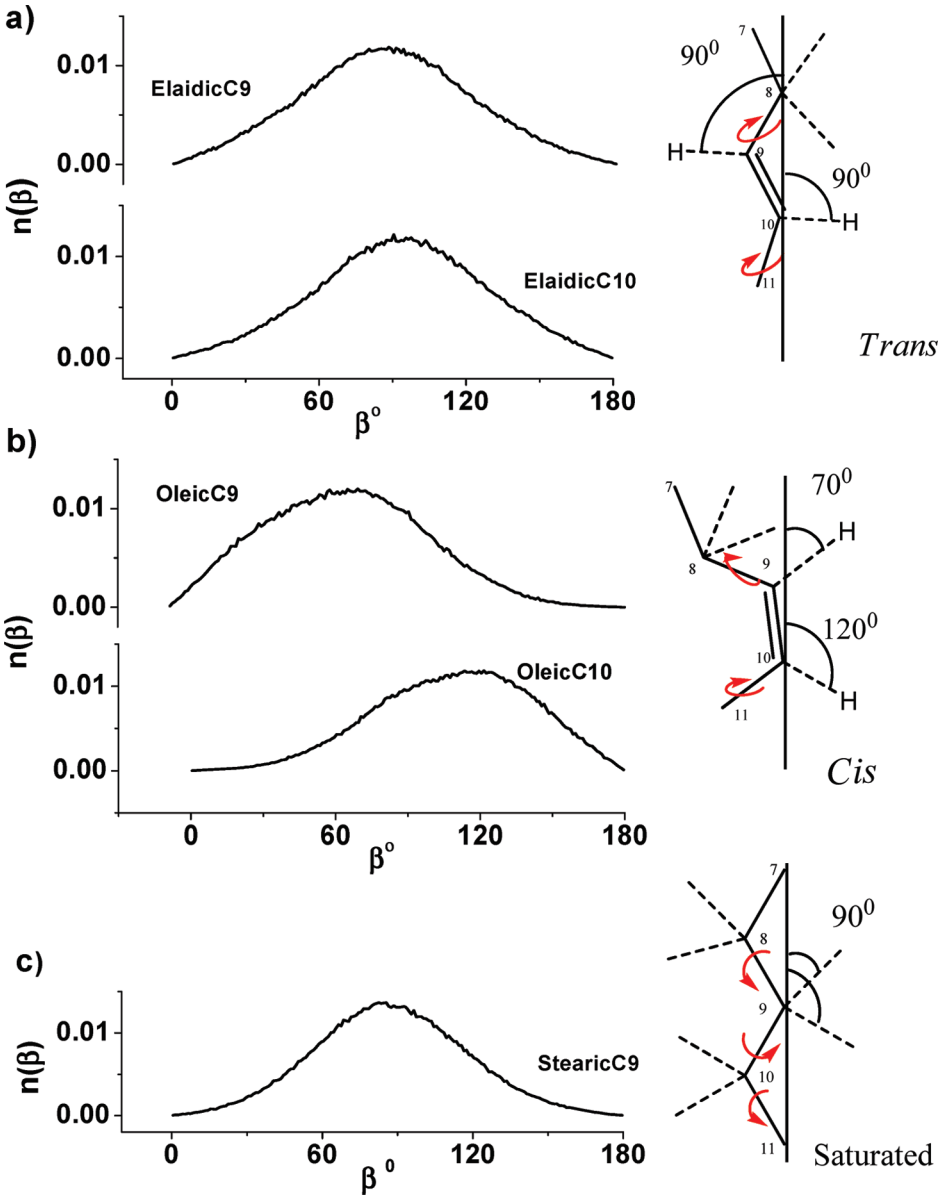

FIGURE 7: Normalized population distribution for the orientation of C−H bonds relative to the bilayer normal calculated from MD simulations for (a) the C9 and C10 positions in the *sn*-1 chain of *t*18:1-18:0PC, (b) the C9 and C10 positions in the *sn*-1 chain of *c*18:1-18:0PC, and (c) the C9 position in the *sn*-2 chain. To the right is a schematic representation of the most probable orientation implied by the maximum in each plot. The arrows indicate where rotations occur between C8 and C11 (H atoms are omitted except on C9 and C10 at the double bond).

We attribute the disordering associated with EA and OA to the reduced energy barrier to rotation for the C−C single bond on each side of a trans (~2.25 kcal/mol) or cis (~1.1 kcal/mol) carbon double bond (vs ~3.5 kcal/mol in a saturated chain) that more than compensates for the rigidity of a double bond. MD simulations that were performed in conjunction with the ^{2}H NMR experiments provide insight. In particular, they reveal details about the motions of the trans and cis double bond in the *sn*-1 chain of *t*18:1-18:0PC and *c*18:1-18:0PC bilayers, respectively, for which we do not have ^{2}H NMR data. Before focusing on the EA and OA *sn*-1 chain, we first established confidence in the simulated data by confirming that the profile of order parameter along the SA *sn*-2 chain generated by simulation (Figure 5b) reproduces the trend seen by NMR (Figure 5a). The quality of agreement is good. The shape of the simulation-obtained profile is characteristic of the saturated chains of phospholipids in the lamellar liquid crystalline phase (*42*). There is a plateau region of slowly varying order in the upper half of the chain that falls off in the lower half of the chain toward the middle of the bilayer. As in the NMR-obtained data, the EA-containing bilayer is slightly more ordered than the OA-containing one, and the difference exists in the lower portion of the chain.

The profiles of order along the EA and OA *sn*-1 chain in the two mono-unsaturated membranes calculated from the MD simulations differ markedly from the saturated SA *sn*-2 chain and from each other (Figure 5c). A largely continuous decrease in S_{CD} values along the whole EA chain toward the terminal methyl group is displayed in the profile for *t*18:1-18:0PC. Either absent or truncated is a plateau region of slowly varying order in the upper portion that characterizes the neighboring SA *sn*-2 chain, and the value of S_{CD} is lower at each position. Like in earlier computer simulations of 16:0-*t*18:1PC (*17*, *18*), there is no major deviation from monotonic variation at the trans double bond which is in stark contrast to the dip in $\bar{S}_{CD}$ values close to the cis double bond observed in the profile for the OA *sn*-1 chain of *c*18:1-18:0PC. The distinction is predominantly attributed to a

different orientation for the trans and cis double bonds rather than a major difference in the extent of the angular fluctuations they undergo. This issue can be understood with the aid of histograms that represent a normalized population distribution for the orientation of C−H bonds relative to the bilayer normal that were calculated from the simulated data generated in this study.

In Figure 7, the distributions of the orientations for the C−H bonds at the C9 and C10 positions in the EA and OA *sn*-1 chains of *t*18:1-18:0PC and *c*18:1-18:0PC, respectively, are plotted. A schematic depiction of the most probable orientation is presented beside each plot. The equivalent information for the C−H bonds on C9 in the SA *sn*-2 chain that is included in the figure serves as a point of reference (Figure 7c). In the case of the saturated chain, the distribution of orientation is approximately symmetric in shape about a most probable angle of $\beta \sim 90°$. The width at half-height of the distribution is ~70°, reflecting the angular range through which the C−H bonds move due to isomerization about C−C bonds along the chain and wobbling of the long molecular axis. Similarly, a distribution of orientation that is approximately symmetric about $\beta \sim 90°$ characterizes the C−H bond on C9 and C10 in the EA *sn*-1 chain (Figure 7a). The curves are essentially identical at the two positions because the C−H bonds are parallel. Their width at half-height, ~80°, is greater than in the SA *sn*-1 chain. We ascribe the additional motion in the unsaturated chain to the reduced energy barrier for rotation about the C−C bonds next to a trans double bond. Unlike either EA or SA, the curves that describe the distribution of orientations for the C−H bond at the C9 and C10 positions in the OA *sn*-1 chain are shifted and asymmetric (Figure 7b). They do not coincide, and ~70° and ~120°, respectively, constitute the most probable orientation. It is the enhanced proportion of orientations near the "magic angle" $\beta = 54°44'$, or its supplemental angle ($180° - \beta$), for which $S_{CD} = 0$ (eq 4) that results in a low order parameter here. As indicated by the width at half-height of the distribution, ~85°, the amplitude of angular fluctuation is not much larger than in the EA chain. This modest increase in the amount of angular motion arises from a further reduction in the energy barrier for rotation around the C−C bonds adjacent to a cis double bond.

Only one direct comparison of molecular organization in EA- and OA-containing membranes has previously been published (*16*). The study by Roach et al. employed a battery of biophysical techniques in comparing PC having TFA and CFA with one or two double bonds. Most closely related to the current discussion were measurements on 18:0-*t*18:1PC versus 18:0-*c*18:1PC of membrane "fluidity" as probed by steady state fluorescence polarization of DPH and AS, and of the area per molecule from pressure−area isotherms for lipid monolayers. Lower fluidity and a smaller area per molecule were found in the trans-unsaturated system, qualitatively agreeing with the higher order seen here for *t*18:1-18:0PC relative to *c*18:1-18:0PC. The modest differential in order between the two unsaturated membranes and the much greater order for saturated 18:0-18:0PC that we detected by ^{2}H NMR (Table 2), however, bely the sweeping assessment made in the earlier study that TFA produce membranes with properties more similar to those of saturated chains than CFA. A more nuanced appraisal is necessary, recognizing that on one hand the conformation of EA somewhat resembles saturated SA while on the other hand EA is dynamically more similar to cis-unsaturated OA.

Over the past decade, it has become generally accepted that lipids are not homogeneously distributed in biological membranes but instead are organized in patches of specific composition to provide the environment that supports the activity of a resident protein (*49*−*51*). Formation of lipid domains is the consequence of unequal affinities between different lipid species or between the lipids and membrane proteins. Lipid rafts make up the domain that has attracted considerable attention (*50*−*52*). They are l_o (liquid ordered) domains enriched in predominantly saturated sphingolipids and cholesterol that are thought to serve as the platform for cell signaling proteins such as GPI-anchored proteins in the outer leaflet of the plasma membrane. At the opposite extreme of rafts are domains formed by polyunsaturated fatty acid (PUFA)-containing phospholipids from which cholesterol is excluded (*53*−*56*). The highly disordered environment in these domains is necessary for the function of certain proteins, notably rhodopsin in the disk membrane of the rod outer segment (*57*), and has been hypothesized to play a central role in the alleviation of a multiplicity of health problems by dietary PUFA (*58*). We, as have others (*9*−*13*, *16*), speculate TFA make up a rogue class of fatty acids that substitute into membrane lipids and locally affect molecular organization to produce a change in protein activity adversely influencing biological function. The possibility that EA may be mistakenly identified as a saturated fatty acid on the basis of its conformation yet disrupts membrane order almost as much as OA is suggested by our results.

CONCLUSION

The picture of the relative effect of trans versus cis unsaturation on molecular organization in a membrane that emerges from our ^{2}H NMR experiments and computer simulations is one in which a trans double bond produces a smaller kink in the linear conformation adopted by a saturated chain than a cis double bond. Thus, there is better chain packing in the gel state and the temperature of the gel to liquid crystalline transition is depressed less for *t*18:1-18:0PC than for *c*18:1-18:0PC. Acyl chain order in the physiologically relevant liquid crystalline phase is reduced almost as much by a trans double bond as by a cis double bond. Average order parameters measured for *t*18:1-18:0PC and *c*18:1-18:0PC coincide within ~7% but are > 25% lower than those for 18:0-18:0PC. The reduction in order relative to the saturated membrane is ascribed to the additional flexibility conferred upon a mono-unsaturated chain by the lower energy barrier to rotation about the single C−C bonds either side of a carbon double bond. We are in the process of synthesizing analogues of *t*18:1-18:0PC deuterated in the EA chain to experimentally examine conformational organization in the region of the trans double bond. In future work, we also plan to investigate how the incorporation of TFA into a membrane affects the interaction of cholesterol.

ACKNOWLEDGMENT

We thank Bruce D. Ray, Daniel S. LoCascio, and Jennifer Runyon for their assistance during synthesis of the deuterated phospholipids.

REFERENCES

1. Sébédio, J. L., and Christie, W. W., Eds. (1998) Trans Fatty Acids in Human Nutrition , The Oily Press, Dundee, Scotland.
2. Stender, S., Dyerberg, J., and Hansen, H. S. (2006) First international symposium on trans fatty acids and health. *Atheroscler. Suppl. 7*, 1–72.
3. Albers, M. J., Harnak, L. J., Steffen, L. M., and Jacobs, D. R. Jr. (2008) 2006 market survey of *trans*-fatty acid content of margarines and butters, cookies and snack cakes, and savory snacks. *J. Am. Diet. Assoc. 108*, 367–370.

4. Allison, D. B., Denke, M. A., Dietschy, J. M., Emken, E. A., Kris-Etherton, P., and Nicolosi, R. J. (1995) Trans fatty acids and coronary heart disease risk. Report of the expert panel on trans fatty acids and coronary heart disease. *Am. J. Clin. Nutr. 62*, 655S–708S.
5. Mozaffarian, D., Katan, M. B., Ascherio, A., Stampfer, M. J., and Willet, W. C. (2006) *Trans* fatty acids and cardiovascular disease. *N. Engl. J. Med. 354*, 1601–1613.
6. Salmeron, J., Hu, F. B., Manson, J. E., Stampfer, M. J., Colditz, G. A., Rimm, E. B., and Willett, W. C. (2001) Dietary fat intake and risk of type 2 diabetes in women. *Am. J. Clin. Nutr. 73*, 1019–1026.
7. Vinikoor, L. C., Schroeder, J. C., Millikan, R. C., Satia, J. A., Martin, C. F., Ibrahim, J., Galanko, J. A., and Sandler, R. S. (2008) Consumption of trans-fatty acid and its association with colorectal adenomas. *Am. J. Epidemiol. 168*, 289–297.
8. Thompson, A. K., Shaw, D. I., Minihane, A. M., and Williams, C. M. (2008) Trans-fatty acids and cancer: The evidence reviewed. *Nutr. Res. Rev. 21*, 174–188.
9. Nui, S. L., Mitchell, D. C., and Litman, B. J. (2005) Trans fatty acid derived phospholipids show increased membrane cholesterol and reduced receptor activation as compared to their cis analogs. *Biochemistry 44*, 4458–4465.
10. Gudheti, M. V., Mlodzianoski, M., and Hess, S. T. (2007) Imaging and shape analysis of giant unilamellar vesicles (GUVs) as model plasma membranes: Effect of trans-DOPC (dielaidoyl phosphatidylcholine) on membrane properties. *Biophys. J. 93*, 2011–2023.
11. Zaloga, G. P., Harvey, K. A., Stillwell, W., and Siddiqui, R. (2006) Trans fatty acids and coronary heart disease. *Nutr. Clin. Pract. 21*, 505–512.
12. Björkbom, A., Ramstedt, B., and Slotte, J. P. (2007) Phosphatidylcholine and sphingomyelin containing an *elaidoyl* fatty acid can form cholesterol-rich lateral domains in bilayer membranes. *Biochim. Biophys. Acta 1768*, 1839–1847.
13. Siddiqui, R. A., Harvey, K., Miller, S. J., and Zaloga, G. (2008) Impact of *omega*-3 and *trans* fatty acids on vascular remodeling: Opposing roles in cardiovascular health. *Curr. Enzyme Inhib. 4*, 60–72.
14. Rey, A., Kolinski, A., Skolnick, J., and Levine, Y. K. (1992) Effect of double bonds on the dynamics of hydrocarbon chains. *J. Chem. Phys. 97*, 1240–1249.
15. Emken, E. A. (1991) Do *trans* acids have adverse health consequences? In Health Effects of Dietary Fatty Acids (Nelson, G. J., Ed.) pp 245−260, AOCS, Champaign, IL.
16. Roach, C., Feller, S. E., Ward, J. A., Shaikh, S. R., Zerouga, M., and Stillwell, W. (2004) Comparison of cis and trans fatty acid containing phosphatidylcholines on membrane properties. *Biochemistry 43*, 6344–6351.
17. Pearce, L. L., and Harvey, S. C. (1993) Langevin dynamics studies of unsaturated phospholipids in a membrane environment. *Biophys. J. 65*, 1084–1092.
18. Rog, T., Murzyn, K., Gurbiel, R., Takaoka, Y., Kusumi, A., and Pasenkiewicz-Gierula, M. (2004) Effects of phospholipid unsaturation on the bilayer nonpolar region: A molecular simulation study. *J. Lipid Res. 45*, 326–336.
19. Linseisen, F., Thewalt, J. L., Bloom, M., and Bayerl, T. M. (1993) ^{2}H-NMR and DSC study of SEPC-cholesterol mixtures. *Chem. Phys. Lipids 65*, 141–149.
20. Holte, L. L., Peter, S. A., Sinnwell, T. M., and Gawrisch, K. (1995) ^{2}H nuclear magnetic resonance order parameter profiles suggest a change of molecular shape for phosphatidylcholines containing a polyunsaturated acyl chain. *Biophys. J. 68*, 2396–2403.
21. Wolf, R. L., Precht, D., and Molkentin, J. (1998) Occurrence and distribution profiles of *trans*-18:1 acids in edible fats of natural origin. In Trans Fatty Acids in Human Nutrition (Sébédio, J. L., Christie, W. W., Eds.) pp 1−33, The Oily Press, Dundee, Scotland.
22. Gennis, R. B. (1989) Biomembranes , Springer-Verlag, New York.
23. Høimer, G. (1998) Biochemistry of *trans*-monoenoic fatty acids. In Trans Fatty Acids in Human Nutrition (Sebedio, J. L., and Christie, W. W., Eds.) pp 163−189, The Oily Press, Dundee, Scotland.
24. Wolff, R. L., and Entressangles, B. (1994) Steady-state fluorescence polarization study of structurally defined phospholipids from liver mitochondria of rats fed elaidic acid. *Biochim. Biophys. Acta 1211*, 198–206.
25. Woldseth, B., Retterstol, K., and Christophersen, B. O. (1998) Monounsaturated trans fatty acids, elaidic acid and trans-vaccenic acid, metabolism and incorporation in phospholipid molecular species in hepatocytes. *Scand. J. Clin. Lab. Invest. 58*, 635–645.
26. Sun, M., Deng, Y., Batyreva, E., Sha, W., and Salomon, R. G. (2002) Novel bioactive phospholipids: Practical total syntheses of products from the oxidation of arachidonic and linoleic esters of 2-lysophosphatidylcholine. *J. Org. Chem. 67*, 3575–3584.
27. McCabe, M. A., and Wassall, S. R. (1997) Rapid deconvolution of NMR powder spectra by weighted fast Fourier transformation. *Solid State Nucl. Magn. Reson. 10*, 53–61.
28. Sternin, E. (1985) Data acquisition and processing: A systems approach. *Rev. Sci. Instrum. 56*, 2043–2049.
29. Davis, J. H., Jeffery, K. R., Bloom, E. T., Valic, M. I., and Higgs, T. P. (1976) Quadrupolar echo deuteron magnetic resonance spectroscopy in ordered hydrocarbon chains. *Chem. Phys. Lett. 42*, 390–394.
30. Davis, J. H. (1983) The description of membrane lipid conformation, order and dynamics by ^{2}H-NMR. *Biochim. Biophys. Acta 737*, 117–171.
31. Lafleur, M., Fine, B., Sternin, E., Cullis, P. R., and Bloom, M. (1989) Smoothed orientational order profile of lipid bilayers by ^{2}H-nuclear magnetic resonance. *Biophys. J. 56*, 1037–1041.
32. Brooks, B. R., Bruccoleri, R. E., Olafson, B. D., States, D. J., Swaminathan, S., and Karplus, M. (1983) CHARMM: A program for macromolecular energy, minimization and dynamics calculation. *J. Comput. Chem. 4*, 187–217.
33. Schlenkrich, M., Brickmann, J., Mackerell, A. D. J., and Karplus, M. (1997) An empirical potential energy function for phospholipids: Criteria for parameter optimization and applications. In Biological Membranes: A Molecular Perspective from Computational and Experiment (Merz, K. M., Jr., and Roux, B., Eds.) pp 31−81, Birkhauser, Boston.
34. Feller, S. E., Yin, D., Pastor, R. W., and MacKerell, A. D. Jr. (1997) Molecular dynamics simulation of unsaturated lipid bilayers at low hydration: Parameterization and comparison with diffraction studies. *Biophys. J. 73*, 2269–2279.
35. Essmann, W., Perera, L., Berkowitz, M. L., Darden, T., Lee, H., and Pedersen, L. G. (1995) A smooth particle mesh Ewald method. *J. Chem. Phys. 103*, 8577–8593.
36. Ryckaert, J. P., Ciccotti, G., and Berendsen, H. J. C. (1977) Numerical intergration of the Cartesian equations of motion of a system with constraint: Molecular dynamics of n-alkanes. *J. Comput. Phys. 103*, 8577–8593.
37. Roark, M., and Feller, S. E. (2009) Molecular dynamics simulation study of correlated motions in phospholipid bilayer membranes. *J. Phys. Chem. B 113*, 13229–13234.
38. Wassall, S. R., Thewalt, J. L., Wong, L., Gorrissen, H., and Cushley, R. J. (1986) Deuterium NMR study of the interaction of α-tocopherol with a phospholipid model membrane. *Biochemistry 25*, 319–326.
39. Engel, A. K., and Cowburn, D. (1981) The origin of multiple quadrupole couplings in the deuterium NMR spectra of the 2 chain of 1,2 dipalmitoyl-*sn*-glycero-3-phosphorylcholine. *FEBS Lett. 126*, 169–171.
40. Scott, H. L. (2002) Modeling the lipid component of membranes. *Curr. Opin. Struct. Biol. 12*, 495–502.
41. Feller, S. E. (2007) Molecular dynamics simulations as a complement to nuclear magnetic resonance and X-ray diffraction measurements. *Methods Mol. Biol. 40*, 89–102.
42. Seelig, J. (1977) Deuterium magnetic resonance: Theory and application to lipid membranes. *Q. Rev. Biophys. 10*, 353–418.
43. Feller, S. E., and MacKerrell, A. D. Jr. (2000) An improved empirical potential energy function for molecular simulations of phospholipids. *J. Phys. Chem. B 104*, 7510–7515.
44. Seelig, J., and Waespe-Sarcevic, N. (1978) Molecular order in cis and trans unsaturated phospholipid bilayers. *Biochemistry 17*, 3310–3315.
45. Seelig, J., Tamm, L., Hymel, L., and Fleischer, S. (1981) Deuterium and phosphorus nuclear magnetic resonance and fluorescence depolarization studies of functional reconstituted sarcoplasmic reticulum membrane vesicles. *Biochemistry 20*, 3922–3932.
46. Chiu, S. W., Jakobsson, E., Subramaniam, S., and Scott, H. L. (1999) Combined Monte Carlo and molecular dynamics simulation of fully hydrated dioleoyl and palmitoyl-oleoyl phosphatidylcholine lipid bilayers. *Biophys. J. 77*, 2462–2469.
47. Huang, C., and Li, S. (1999) Calorimetric and molecular mechanics studies of the thermotropic phase behavior of membrane phospholipids. *Biochim. Biophys. Acta 1422*, 273–307.
48. Schindler, H., and Seelig, J. (1975) Deuterium order parameters in relation to thermodynamic properties of a phospholipid bilayer. A statistical mechanical interpretation. *Biochemistry 14*, 2283–2287.
49. Jacobson, K., Sheets, E. D., and Simson, R. (1995) Revisiting the fluid mosaic model of membranes. *Science 268*, 1441–1442.
50. Simons, K., and Ikonen, E. (1997) Functional rafts in cell membranes. *Nature 387*, 569–572.
51. Edidin, M. (2003) The state of lipid rafts: From model membranes to cells. *Annu. Rev. Biophys. Biomol. Struct. 32*, 257–283.
52. Brown, D. A., and London, E. (2000) Structure and function of sphingolipid and cholesterol-rich membrane rafts. *J. Biol. Chem. 275*, 17221–17224.

53. Huster, D., Arnold, K., and Gawrisch, K. (1998) Influence of docosahexaenoic acid and cholesterol on lateral lipid organization in phospholipid mixtures. *Biochemistry 37*, 17299–17308.
54. Mitchell, D. C., and Litman, B. J. (1998) Molecular order and dynamics in bilayers consisting of highly polyunsaturated phospholipids. *Biophys. J. 74*, 879–891.
55. Shaikh, S. R., and Edidin, M. A. (2006) Membranes are not just rafts. *Chem. Phys. Lipids 144*, 1–3.
56. Wassall, S. R., and Stillwell, W. (2008) Docosahexaenoic acid domains: The ultimate non-raft membrane domain. *Chem. Phys. Lipids 153*, 57–63.
57. Polozova, A., and Litman, B. J. (2000) Cholesterol dependent recruitment of di22:6-PC by a G protein-coupled receptor into lateral domains. *Biophys. J. 79*, 2632–2643.
58. Wassall, S. R., and Stillwell, W. (2009) Polyunsaturated fatty acid-cholesterol interactions: Domain formation in membranes. *Biochim. Biophys. Acta 1788*, 24–32.